VI International Conference on Computational Methods for Coupled Problems in Science and Engineering
COUPLED PROBLEMS 2015
B. Schrefler, E. Oñate and M. Papadrakakis(Eds)

A CONSERVATIVE, OPTIMIZATION-BASED SEMI-LAGRANGIAN SPECTRAL ELEMENT METHOD FOR PASSIVE TRACER TRANSPORT

Pavel B. Bochev*, Scott A. Moe†, Kara J. Peterson* and Denis Ridzal**

*Computational Mathematics,
Sandia National Laboratories[1], Mail Stop 1320
Albuquerque, New Mexico, 87185-1320.

**Optimization and Uncertainty Quantification,
Sandia National Laboratories, Mail Stop 1320
Albuquerque, New Mexico, 87185-1320.

†University of Washington
Department of Applied Mathematics
Seattle, WA 98195

Key words: High order methods, transport, semi-Lagrangian methods, optimization

Abstract. We present a new optimization-based, conservative, and quasi-monotone method for passive tracer transport. The scheme combines high-order spectral element discretization in space with semi-Lagrangian time stepping. Solution of a singly linearly constrained quadratic program with simple bounds enforces conservation and physically motivated solution bounds. The scheme can handle efficiently a large number of passive tracers because the semi-Lagrangian time stepping only needs to evolve the grid points where the primitive variables are stored and allows for larger time steps than a conventional explicit spectral element method. Numerical examples show that the use of optimization to enforce physical properties does not affect significantly the spectral accuracy for smooth solutions. Performance studies reveal the benefits of high-order approximations, including for discontinuous solutions.

[1]Sandia National Laboratories is a multi-program laboratory managed and operated by Sandia Corporation, a wholly owned subsidiary of Lockheed Martin Corporation, for the U.S. Department of Energy's National Nuclear Security Administration under contract DE-AC04-94AL85000.

1 INTRODUCTION

In this paper we present a semi-Lagrangian spectral element method (SL-SEM) for the solution of the scalar transport equation for a positive density function ρ,

$$\frac{\partial \rho}{\partial t} + \nabla \cdot (\boldsymbol{v}\rho) = 0, \tag{1}$$

and the related equation

$$\frac{\partial \rho q}{\partial t} + \nabla \cdot \rho q \boldsymbol{v} = 0 \tag{2}$$

for transport of a passive tracer with mixing ratio q. Equations (1)–(2) imply that

$$\frac{\partial q}{\partial t} + \boldsymbol{v} \cdot \nabla q = 0\,, \tag{3}$$

that is, the passive tracer is constant along the characteristics. Although (3) is relatively simple, atmospheric models may involve large numbers of passive tracers, which makes their solution a major part of the computational cost.

The use of SEM for the spatial discretization of (3) offers important computational advantages such as a diagonal mass matrix and arbitrary order of accuracy [9]. However, in combination with an explicit time stepping scheme SEM, like other high-order methods, suffers from a severe, stability imposed, time step restriction.

On the other hand, schemes that adopt a Lagrangian viewpoint [3] and directly approximate the motion of "fluid particles" under a given velocity field have the potential to avoid restrictive CFL stability conditions. This makes such time stepping schemes particularly attractive for use with high-order spatial discretizations; see, e.g., [4, 11, 5] for some recent efforts to combine SEM with semi-Lagrangian time stepping.

An important complaint, though, about SL-SEM schemes is that they do not necessarily preserve physical properties such as conservation of total mass, or local solution bounds. Yet, such properties are often critical for accurate and physically consistent simulations of atmospheric models. This is especially true for schemes employing high-order spatial discretizations because in the presence of solution discontinuities such methods are prone to large unphysical oscillations, known as Runge or Gibbs phenomena.

In this work we combine the attractive traits of a *parent* SL-SEM with a novel, optimization-based strategy for the enforcement of the relevant physical properties [1]. Specifically, the raw high-order solution of the SL-SEM defines an *optimization* target, whereas mass conservation and physically motivated local solution bounds provide the optimization constraints. The actual solution is then determined by solving a singly linearly constrained quadratic program with simple bounds, which can be done very efficiently [2]. Similar ideas have been applied in an Eulerian spectral element method [6], however in the context of explicit time stepping. Our approach allows for the same high-order accuracy but avoids the stringent time stepping restriction experienced in that work.

2 PRELIMINARIES

2.1 Scalar advection

The basic problem considered in this work is the numerical solution of the multi-dimensional scalar advection equation (3). Atmospheric models require simultaneous advection of many tracers, which makes this problem a major source of computational cost. A semi-Lagrangian method would be ideal for this for two reasons. First it would allow much larger time steps than an Eulerian method. Second, to advect multiple tracer values located at a grid point, the method moves that point along a characteristic line and then computes the updated solution by interpolating the tracer values at the new point location. As a result, the cost to track the characteristics is amortized over a large number of passive tracer values.

This work focuses on divergence-free velocity fields. In this case equation (1) has the same form as (3), and $\int_\Omega q dV$ is a conserved quantity. Thus, we present the method for (3) alone. Formulations for general velocities will be considered in a forthcoming paper.

2.2 Spatial discretization

In this work we combine spatial discretization by spectral elements with semi-Lagrangian time stepping. For simplicity we describe the approach in two dimensions. Extension of the main ideas to three dimensions is straightforward. Thus, in what follows $K(\Omega)$ is a conforming partition of a bounded region $\Omega \in \mathbf{R}^2$ into quadrilateral cells κ_i, $i = 1, \ldots, K$.

In the spectral element method the basis functions on the reference quadrilateral $\hat{\kappa} = [-1, 1]^2$ are Lagrange polynomials corresponding to a tensor product grid of Gauss-Legendre-Lobatto (GLL) nodes. Specifically, let $\mathcal{N} = \{\xi_i\}_{i=1}^{r+1}$ denote a set of GLL nodes in $[-1, 1]$ and let

$$\hat{X} = \{(\xi_i, \xi_j) \,|\, \xi_i, \xi_j \in \mathcal{N}\}$$

be the corresponding GLL tensor product grid in $\hat{\kappa}$. The associated reference spectral element basis functions $\{\hat{\phi}_{ij}\}$ are rth degree Lagrange polynomials such that

$$\hat{\phi}_{ij}(\xi_l, \xi_k) = \delta_{li}\delta_{kj} \,. \tag{4}$$

Given an element $\kappa_m \in K(\Omega)$, let F_m be the isoparametric map defined by (4), which takes the reference element into κ_m, i.e., $F_m(\hat{\kappa}) = \kappa_m$. The image of $\hat{X}$ under F_m

$$X^m = \{\boldsymbol{x}_{ij} = F_m(\xi_i, \xi_j) \,|\, \xi_i, \xi_j \in \mathcal{N}\}$$

provides a GLL tensor product grid on κ_m. We define the spectral element basis $\{\phi_{kl}\}$ on $K(\Omega)$ by pullback, i.e., the local basis set $\{\phi_{ij}^m\}_{i=1}^{r+1}$ on an element κ_m comprises the functions

$$\phi_{ij}^m(\boldsymbol{x}) = \hat{\phi}_{ij} \circ F_m^{-1}(\boldsymbol{x}) \,.$$

The spectral element space $\mathbb{Q}^r = \text{span}\{\phi_{kl}\}$. Although the accuracy of the GLL nodes is slightly less than that of Gauss-Legendre nodes ($2r - 1$ vs. $2r + 1$ for $r + 1$ points), the use of the former brings about some very attractive computational properties.

- They display asymptotically optimal Lebesgue Constant growth [10].
- The associated GLL quadrature does not significantly degrade the accuracy of the discrete solution.
- The basis (4) is orthogonal with respect to the GLL points, which results in a diagonal mass matrix when using them as quadrature points for SEM.
- Inclusion of the endpoints of the interval allows to maintain inter-element continuity.

The ability to maintain inter-element continuity is important for the stability of the spectral element method. For instance, using Gauss-Legendre nodes to implement a semi-Lagrangian scheme may introduce large oscillations due to solution discontinuities across element interfaces. For brevity, we restrict attention to bi-cubic basis functions $\hat{\phi}_{ij}$. In this case the relevant set $\mathcal{N}$ contains the following four GLL nodes:

$$X = \left\{-1, -\sqrt{1/5}, \sqrt{1/5}, 1\right\} \tag{5}$$

2.3 A parent semi-Lagrangian spectral element method (SL-SEM)

Let $\tilde{\boldsymbol{x}}(t)$ be the solution of the characteristic equation

$$\frac{d\tilde{\boldsymbol{x}}}{dt} = \boldsymbol{v} \quad \text{and} \quad \tilde{\boldsymbol{x}}(0) = \tilde{\boldsymbol{x}}_0, \tag{6}$$

and let $q(\boldsymbol{x}, t)$ be a solution of (3). Then,

$$\frac{d}{dt} q(\tilde{\boldsymbol{x}}(t), t) = \frac{\partial q}{\partial t} + \frac{d\tilde{\boldsymbol{x}}}{dt} \cdot \nabla q = \frac{\partial q}{\partial t} + \boldsymbol{v} \cdot \nabla q = 0. \tag{7}$$

In other words, q is constant along the characteristics $\tilde{\boldsymbol{x}}(t)$. Thus, if q is known at $\tilde{\boldsymbol{x}}(0)$ its values along $\tilde{\boldsymbol{x}}(t)$ can be determined by tracking the characteristic line. This observation forms the basis of semi-Lagrangian methods.

2.3.1 Semi-Lagrangian time stepping scheme

The semi-Lagrangian approach solves equation (3) by breaking it up into a series of ODEs of the form (6) coupled with an interpolation. To describe the basic scheme let X be the union of all GLL points in the mesh $K(\Omega)$, i.e., $X = \cup_{\kappa_m} X^m$. Suppose that the values of q at the current time step t_n are known at all points in X. To find the approximation of q at the GLL points at $t_{n+1} = t_n + \Delta t$ we track these points back along the characteristic lines using X as initial data for (6). Succinctly, the two steps are

$$\begin{aligned} &\text{Trace back:} \quad \forall \boldsymbol{x}_{ij} \in X \ \text{ solve: } \ \frac{d\tilde{\boldsymbol{x}}_{ij}}{dt} = -\boldsymbol{v} \ \text{ in } \ [t_n, t_{n+1}] \quad \text{with} \quad \tilde{\boldsymbol{x}}_{ij}(t_n) = \boldsymbol{x}_{ij}, \\ &\text{Interpolate:} \quad q(\boldsymbol{x}_{ij}, t_{n+1}) := q(\tilde{\boldsymbol{x}}_{ij}(t_{n+1}), t_n). \end{aligned} \tag{8}$$

The point $\tilde{\boldsymbol{x}}_{ij}(t_{n+1})$ is generally referred to as the "trace back" of the GLL point $\boldsymbol{x}_{ij} \in X$. In a nutshell, the parent semi-Lagrangian scheme transports the function q back along the characteristics and then uses the spectral element basis to interpolate its value at $\tilde{\boldsymbol{x}}_{ij}(t_{n+1})$; see Figure 2.3.1.

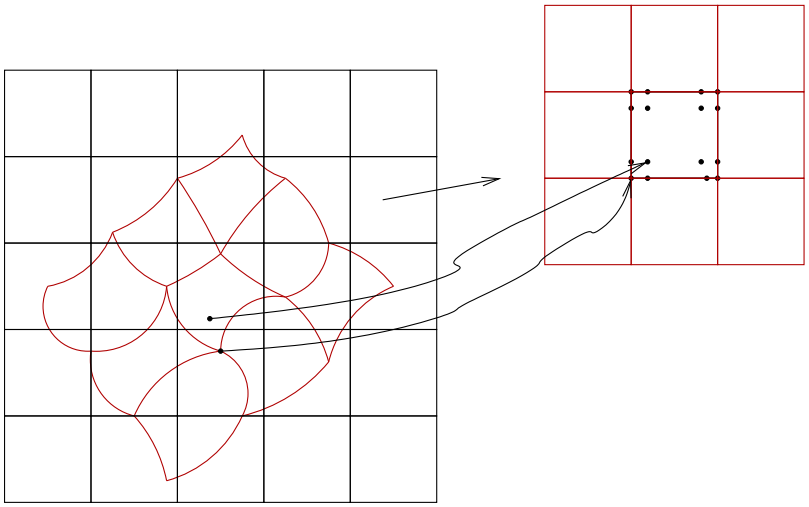

Figure 1: The SL-SEM traces back the GLL set along the characteristics $\tilde{\boldsymbol{x}}(t)$ and then uses the spectral basis to interpolate $q(\tilde{\boldsymbol{x}}(t_{n+1}), t_n)$. The interpolated values provide the approximation $q(\boldsymbol{x}_{ij}, t_{n+1})$ of q at the GLL points *at the next time step.*

Although formally of high-order, the parent SL-SEM does not preserve local solution bounds. A simple solid body rotation example illustrates this fact and motivates the need for an optimization-based solution to preserve relevant physical properties. Specifically, we apply the SL-SEM to advect a discontinuous profile given by the slotted Zalesak cylinder [7] using the rotational velocity field

$$\boldsymbol{v} = \begin{bmatrix} (0.5 - y) & (0.5 - x) \end{bmatrix}^T. \tag{9}$$

The velocity field (9) rotates the initial profile around the center of the unit square with period 2π. There is no deformation and the velocity field is divergence free.

Figure 2(b) compares the initial profile with the SL-SEM solution after one full revolution. The exact solution satisfies global solution bounds and should remain between 0 and 1. The side view in Figure 2(c) clearly shows that the numerical solution develops spurious oscillations and significantly violates the global solution bounds.

3 OPTIMIZATION-BASED SL-SEM

In this section we combine the SL-SEM with an optimization-based approach to enforce conservation and local solution bounds. We note that in Eulerian methods preservation of

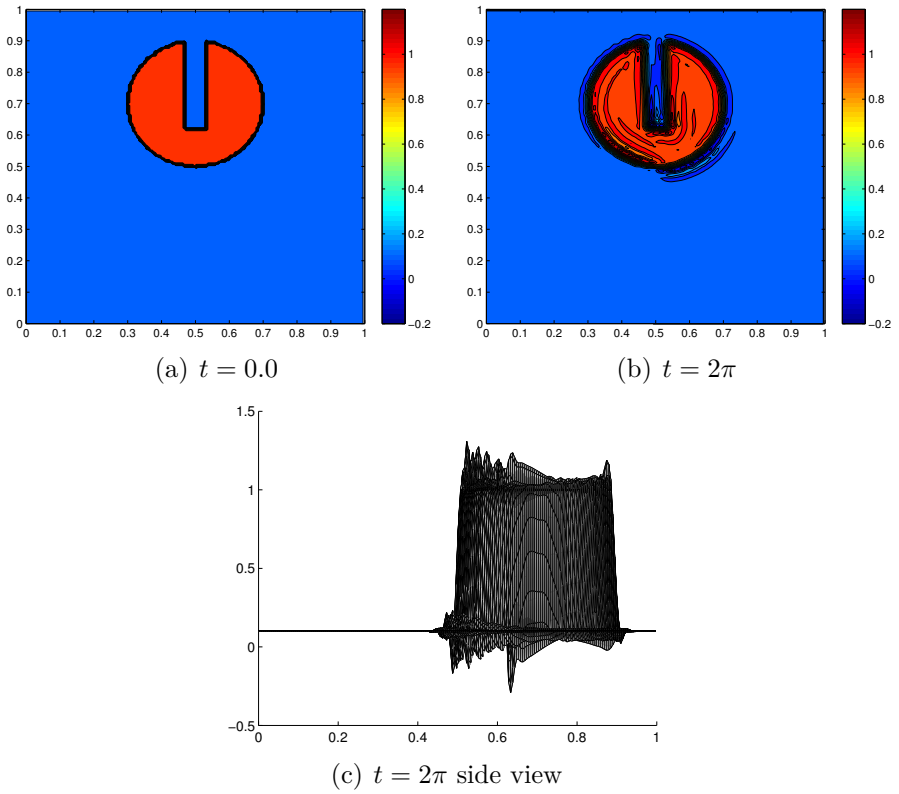

(a) $t = 0.0$ (b) $t = 2\pi$

(c) $t = 2\pi$ side view

Figure 2: SL-SEM solution of the solid body rotation problem with a slotted cylinder initial condition on an 80×80 uniform grid with $CFL = 0.7$. (a) Initial profile; (b) solution after one revolution; (c) side view after one revolution. The discontinuous initial profile results in spurious oscillations.

local bounds is accomplished through the use of limiters to obtain monotone reconstructions of the primitive variables. This prevents the numerical solution from developing new extrema.

The theory of monotonicity preserving limiters is well understood and developed for low-order finite volume methods [8]. However, because limiters modify the reconstruction process their application to high-order methods may degrade the accuracy. In fact, for such methods it is not clear how to preserve monotonicity without harming accuracy in smooth regions, or even if that is possible.

In contrast, following the ideas of [1] we separate reconstruction from the enforcement of physical properties such as solution bounds and conservation. To this end, we treat the solution of the parent SL-SEM as an optimization target, whereas the local solution bounds and mass conservation define the optimization constraints. The goal is to find the spectral element function that is the closest to the target field and simultaneously satisfies the constraints.

In particular, one can enforce bounds on the interpolation operator itself, giving completely decoupled bounds for each individual degree of freedom. Because the type of lower

and upper bounds introduced are not guaranteed to enforce exact monotonicity, we refer to this type of methods as *quasi-monotone* [6].

Optimization-based SL-SEM. Given SEM approximation $q_n(\boldsymbol{x}) \approx q(\boldsymbol{x}, t_n)$ the following algorithm computes the optimization-based SL-SEM solution $q_{n+1}(\boldsymbol{x}) \approx q(\boldsymbol{x}, t_{n+1})$ at the next time step:

1. Trace back: $\forall \boldsymbol{x}_{ij} \in X$ solve: $\dfrac{d\tilde{\boldsymbol{x}}_{ij}}{dt} = -\boldsymbol{v}$ in $[t_n, t_{n+1}]$ with $\tilde{\boldsymbol{x}}_{ij}(t_n) = \boldsymbol{x}_{ij}$.
2. Interpolate and set target: $\tilde{q}_{n+1}(\boldsymbol{x}_{ij}) := q_n(\tilde{\boldsymbol{x}}_{ij}(t_{n+1}))$.
3. Determine lower and upper bounds $\underline{q}_{ij}$ and $\overline{q}_{ij}$, respectively for $q_{n+1}(\boldsymbol{x}_{ij})$.
4. Determine $q_{n+1}(\boldsymbol{x})$ by solving the optimization problem:

$$q_{n+1} = \arg\min_{q \in \mathbb{Q}^r} \|q - \tilde{q}_{n+1}\|_0^2 \quad \text{subject to} \begin{cases} \int_\Omega q d\Omega = \int_\Omega q_n d\Omega & \text{(Conservation)} \\ \underline{q}_{ij} \le q(\boldsymbol{x}_{ij}) \le \overline{q}_{ij} & \text{(Local bounds)} \end{cases} \tag{10}$$

3.1 Determination of local solution bounds

Because the solution is constant along the characteristic lines, we can determine $\underline{q}_{ij}$ and $\overline{q}_{ij}$ by examining solution values in a neighborhood of the trace back point $\tilde{\boldsymbol{x}}_{ij}(t_{n+1})$. In this paper we adopt an approach where these bounds are set by computing the minimum and maximum solution values at the GLL points in the neighborhood of the element containing $\tilde{\boldsymbol{x}}_{ij}(t_{n+1})$. Given $\kappa_i \in K(\Omega)$ let $B(\kappa_i)$ be the set of all its neighbors and κ_i itself.

Local solution bounds. Given a trace back point $\tilde{\boldsymbol{x}}_{ij}(t_{n+1})$ the following procedure determines local solution bounds for the optimization-based SL-SEM:

1. Find element $\kappa_m \in K(\Omega)$ such that $\tilde{\boldsymbol{x}}_{ij}(t_{n+1}) \in \kappa_m$.
2. Define $\chi_m = \{\boldsymbol{x}_{kl} | \boldsymbol{x}_{kl} \in X \text{ and } \boldsymbol{x}_{kl} \in B(\kappa_m)\}$.
3. Set bounds $\underline{q}_{ij} = \min_{\boldsymbol{x} \in \chi_m} q_n(\boldsymbol{x})$ and $\overline{q}_{ij} = \max_{\boldsymbol{x} \in \chi_m} q_n(\boldsymbol{x})$.

3.2 Algebraic form of the optimization problem

For notational simplicity we drop the time step index from the target and simply write $\tilde{q}$. The coefficient vectors of $\tilde{q}$ and the state q are denoted by $\tilde{\mathbf{q}}$ and $\mathbf{q}$, respectively. Expanding the objective yields

$$\|q - \tilde{q}\|_0^2 = \sum_{i,j=1}^{r+1} \sum_{k,l=1}^{r+1} (q_{ij} q_{kl} - 2 q_{ij} \tilde{q}_{kl} + \tilde{q}_{ij} \tilde{q}_{kl}) \int_\Omega \phi_{ij} \phi_{kl} d\Omega, \tag{11}$$

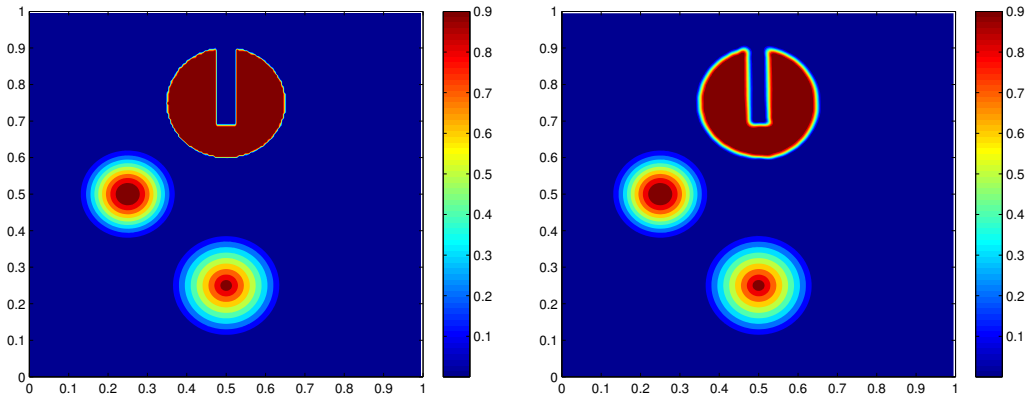

(a) $t = 0.0$ (b) $t = 2\pi$

Figure 3: Optimization-based SL-SEM solution of the solid body rotation problem with initial profiles of varying degrees of smoothness; 100×100 uniform grid, bi-cubic elements, and CFL=0.7. (a) Initial time; (b) Solution after one full revolution.

where ϕ_{ij} are the spectral basis functions corresponding to the GLL nodes in X. Thus,

$$\|q - \tilde{q}\|_2^2 = \mathbf{q}^T M \mathbf{q} + \mathbf{c}^T \mathbf{q} + \mathbf{c}_0; \quad \mathbf{c} = -2M\tilde{\mathbf{q}}; \quad \mathbf{c}_0 = \tilde{\mathbf{q}}^T M \tilde{\mathbf{q}} \quad \text{and} \quad M_{ij,kl} = \int_\Omega \phi_{ij}\phi_{kl} d\Omega.$$

The SEM approximates the integrals above by using the GLL points in X along with suitable weights $\{w_{ij}\}$. Let $\mathbf{w}$ be the vector of these weights. Since the SEM basis functions are orthogonal with respect to the GLL nodes it follows that $M = diag(w_{ij}) = \mathbf{w}$. As a result, the SL-SEM optimization problem (10) assumes the following simple algebraic form

$$\mathbf{q}_{n+1} = \arg\min_{\mathbf{q}} \mathbf{q}^T M \mathbf{q} + \mathbf{c}^T \mathbf{q} + \mathbf{c}_0 \quad \text{subject to} \quad \begin{cases} \mathbf{w}^T \mathbf{q} = \mathbf{w}^T \mathbf{q}_n & \text{(Conservation)} \\ \underline{\mathbf{q}} \le \mathbf{q} \le \overline{\mathbf{q}} & \text{(Local bounds)} \end{cases} \tag{12}$$

Problem (12) is a singly linearly constrained quadratic program (QP) with simple bounds. The structure of this QP lends itself to an extremely efficient solution method; see [2].

4 NUMERICAL EXAMPLES

4.1 Solid body rotation test

To test the optimization-based SL-SEM we combine the rotational velocity field from Section 2.3.1 with an initial profile comprising a notched cylinder, a smooth hump and a cone. This example is a standard advection test introduced in [7]. Figure 3 shows the initial profile and the numerical solution after one full revolution. The plot in Fig.3(b) reveals minimal smearing of the discontinuous profiles and an essentially monotone solution.

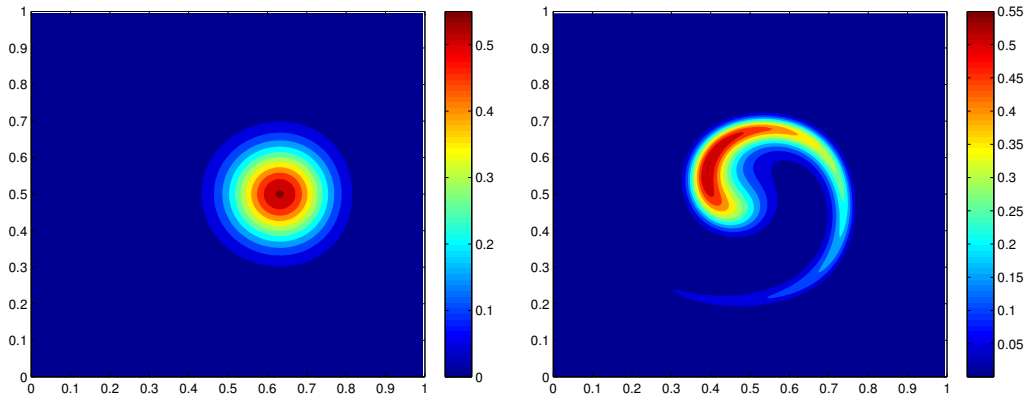

(a) $t = 0.0$ (b) $t = 2.5$

Figure 4: Optimization-based SL-SEM solution of the modified deformational flow example using 80×80 uniform grid and bi-cubic basis functions. (a) Initial profile; (b) Solution at maximum deformation time.

4.2 Modified deformational flow test

This example uses a modified version of the deformational flow test on the sphere, which is standard in the climate modeling community [6]. The goal is to examine the convergence rates of the optimization-based SL-SEM. Specifically, we combine the divergence-free velocity field $\boldsymbol{v} = \begin{bmatrix} u & v \end{bmatrix}^T$ where

$$\begin{aligned} u &= \sin(\pi x)\sin(\pi x)\sin(2\pi y)\cos\left(\pi\frac{t}{T}\right) \\ v &= -\sin(\pi y)^2\sin(2\pi x)\cos\left(\pi\frac{t}{T}\right) \end{aligned} \tag{13}$$

with a Gaussian initial profile defined on $\Omega = [0,1] \times [0,1]$ by

$$q(x_1, x_2) = \sin(2\pi x)^4 \sin(2\pi y)^4 \exp\left(-\beta((x_1 - x_0)^2 + (x_2 - y_0)^2)\right) \tag{14}$$

where $\beta = -40.0$ and $(x_0, y_0) = (0.7, 0.5)$. The velocity field is designed so that after time $t = 2.5$ it reverses and the profile returns to the initial condition at 5.0. The initial profile is infinitely smooth except for the boundary where it is scaled so that it is zero on $\partial\Omega$. This allows us to impose periodic boundary conditions.

Figure 4 shows the initial profile and the solution at the maximum deformation instant $t = 2.5$. Figure 5 shows the convergence results for this example. We observe a slight degradation in the accuracy of the L_∞ norm errors, while the L_1-norm errors are not significantly affected. This is a very good result for a method that also eliminates oscillations. A method that is exactly monotonicity preserving would typically truncate the convergence rate to order 2 even in the L_1 norm.

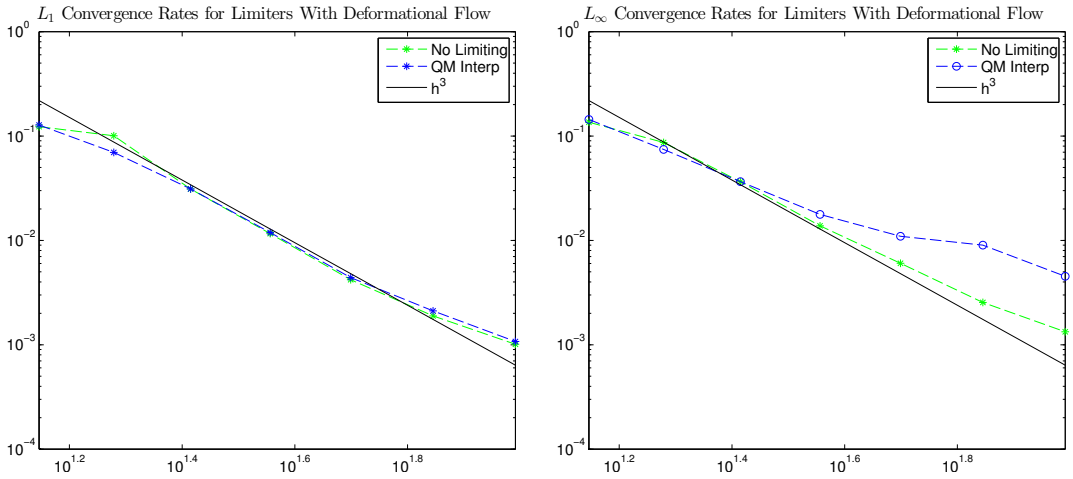

(a) The L_1 norm convergence rate (b) The L_∞ norm convergence rate

Figure 5: The effect of optimization-based enforcement of local bounds on convergence rates.

5 PERFORMANCE STUDIES

This section compares several realizations of the optimization-based SL-SEM with different orders of basis functions. The comparison is done using a Gaussian profile and the slotted Zalesak cylinder both advected by the deformational flow velocity field introduced in Section 4.2. In all cases we use fourth-order Runge Kutta for back-tracing the characteristics.

In this study the SL-SEM is run over a wide range of mesh and time step sizes using several different polynomial orders. The purpose of this study is to examine the accuracy of the method as a function of the spatial resolution, as measured by the number of spatial degrees of freedom and the temporal resolution, determined by a varying time step size. The accuracy is measured by the L_2-norm error. Figures 6(a) and 6(b) reveal an interesting behavior of the optimization-based SL-SEM. Unlike with Eulerian schemes, there is an optimal time step size. The reason for this is that every interpolation instance builds up some amount of error. Thus, there appears to be an optimal time step size which balances the accumulation of the errors with the available resolution. Also, as expected, increasing the number of spatial degrees of freedom tends to reduce errors.

All numerical computations in this section are done on a workstation with an Intel core i5-2500 processor and 8 Gigabytes of memory.

6 CONCLUSIONS

We presented an optimization-based semi-Lagrangian spectral element method for a scalar advection equation. The method combines a characteristic-based approach with optimization to enforce preservation of physical properties such as global conservation and local solution bounds. Convergence studies reveal minimal degradation of L_1-norm

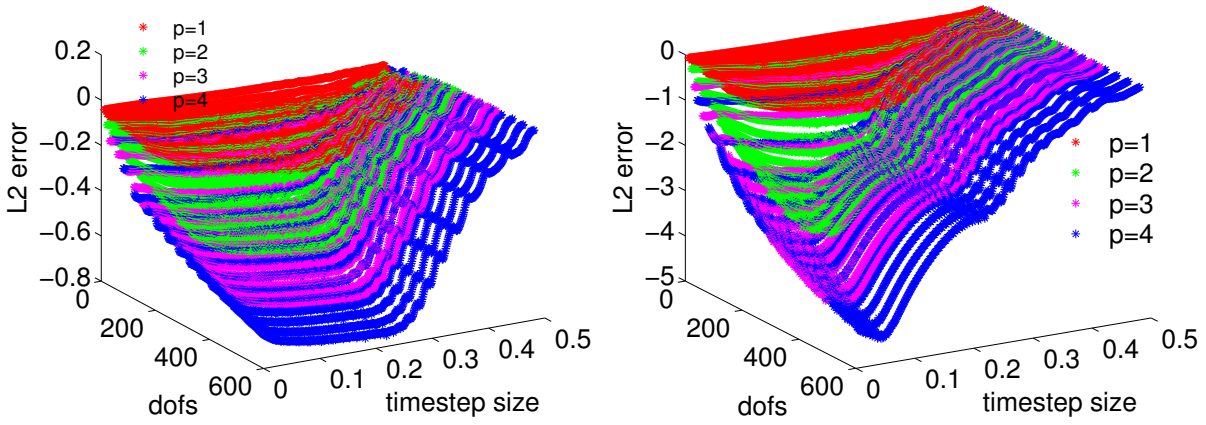

(a) Discontinuous initial condition

(b) Gaussian initial condition

Figure 6: Parameter study of the approximation error in the optimization-based SL-SEM as function of the time step size and the number of spatial degrees-of-freedom for different polynomial degrees.

convergence rate for smooth solutions.

A parameter study was performed to characterize accuracy with respect to the number of degrees of freedom and the time step size. The study reveals the existence of an optimal time step for a given spatial resolution and indicates that higher polynomial degrees outperform lower degrees even on discontinuous profiles, which confirms the utility of the proposed approach in the context of high-order approximations.

Acknowledgements

This material is based upon work supported by the U.S. Department of Energy, Office of Science, Office of Advanced Scientific Computing Research.

REFERENCES

[1] Pavel Bochev, Denis Ridzal, and Kara Peterson. Optimization-based remap and transport: A divide and conquer strategy for feature-preserving discretizations. *Journal of Computational Physics*, 257:1113–1139, 2014.

[2] Pavel Bochev, Denis Ridzal, and Mikhail Shashkov. Fast optimization-based conservative remap of scalar fields through aggregate mass transfer. *Journal of Computational Physics*, 246(0):37 – 57, 2013.

[3] Jim Douglas, Jr and Thomas F Russell. Numerical methods for convection-dominated diffusion problems based on combining the method of characteristics with finite element or finite difference procedures. *SIAM Journal on Numerical Analysis*, 19(5):871–885, 1982.

[4] Francis X Giraldo. The Lagrange–Galerkin spectral element method on unstructured quadrilateral grids. *Journal of Computational Physics*, 147(1):114–146, 1998.

[5] FX Giraldo, JB Perot, and PF Fischer. A spectral element semi-Lagrangian (sesl) method for the spherical shallow water equations. *Journal of Computational Physics*, 190(2):623–650, 2003.

[6] Oksana Guba, Mark Taylor, and Amik St-Cyr. Optimization-based limiters for the spectral element method. *Journal of Computational Physics*, 267:176–195, 2014.

[7] Randall J. LeVeque. High-resolution conservative algorithms for advection in incompressible flow. *SIAM Journal on Numerical Analysis*, 33(2):627–665, 1996.

[8] Randall J LeVeque. *Finite volume methods for hyperbolic problems*, volume 31. Cambridge university press, 2002.

[9] MA Taylor, J Edwards, S Thomas, and R Nair. A mass and energy conserving spectral element atmospheric dynamical core on the cubed-sphere grid. In *Journal of Physics: Conference Series*, volume 78, page 012074. IOP Publishing, 2007.

[10] Lloyd N Trefethen. *Approximation theory and approximation practice*. Siam, 2013.

[11] Dongbin Xiu and George Em Karniadakis. A semi-Lagrangian high-order method for Navier–Stokes equations. *Journal of computational physics*, 172(2):658–684, 2001.